Journal Pre-proof

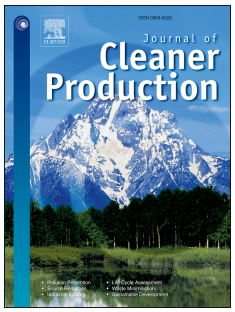

Catalytic degradation of waste rubbers and plastics over metal-modified HY zeolites to produce aromatic hydrocarbons

Jia Wang, Jianchun Jiang, Yunjuan Sun, Xiaobo Wang, Mi Li, Shusheng Pang, Roger Ruan, Arthur J. Ragauskas, Yong Sik Ok, Daniel C.W. Tsang

PII: S0959-6526(21)01688-7

DOI: https://doi.org/10.1016/j.jclepro.2021.127469

Reference: JCLP 127469

To appear in: *Journal of Cleaner Production*

Received Date: 5 January 2021

Revised Date: 23 April 2021

Accepted Date: 6 May 2021

Please cite this article as: Wang J, Jiang J, Sun Y, Wang X, Li M, Pang S, Ruan R, Ragauskas AJ, Ok YS, Tsang DCW, Catalytic degradation of waste rubbers and plastics over metal-modified HY zeolites to produce aromatic hydrocarbons, *Journal of Cleaner Production*, https://doi.org/10.1016/j.jclepro.2021.127469.

Credit Author Statement

Jia Wang: Conceptualization, Methodology, Investigation, Data curation, Writing - Original draft preparation.

Jianchun Jiang: Conceptualization, Supervision, Project administration, Resources, Funding acquisition, Writing - Review & Editing.

Xiaobo Wang: Investigation, Formal analysis, Data curation.

Mi Li: Writing - Review & Editing.

Yunjuan Sun: Validation.

Shusheng Pang: Validation, Formal analysis.

Roger Ruan: Validation, Writing - Review & Editing.

Arthur J. Ragauskas: Conceptualization, Project administration, Writing - Review & Editing.

Yong Sik Ok: Validation, Supervision, Project administration.

Daniel C.W. Tsang: Conceptualization, Supervision, Validation, Resources, Funding acquisition, Writing - Review & Editing.

Catalytic degradation of waste rubbers and plastics over metal-modified HY zeolites to produce aromatic hydrocarbons

Jia Wang [a, b], *Jianchun Jiang* [a, b*], *Yunjuan Sun* [b], *Xiaobo Wang* [c], *Mi Li* [d], *Shusheng Pang* [e], *Roger Ruan* [f], *Arthur J. Ragauskas* [d, g, h], *Yong Sik Ok* [i], *Daniel C.W. Tsang* [j*]

[a] *Jiangsu co-Innovation Center for Efficient Processing and Utilization of Forest Resources, College of Chemical Engineering, Nanjing Forestry University, Longpan Road 159, Nanjing 210037, China*

[b] *Institute of Chemical Industry of Forest Products, Chinese Academy of Forestry (CAF), No. 16, Suojin Five Village, Nanjing 210042, China*

[c] *School of Environmental Science, Nanjing Xiaozhuang University, Nanjing 211171, China*

[d] *Center for Renewable Carbon, Department of Forestry, Wildlife and Fisheries, The University of Tennessee, Knoxville, TN 37996, USA*

[e] *Department of Chemical and Process Engineering, University of Canterbury, Christchurch, New Zealand*

[f] *Center for Biorefining and Department of Bioproducts and Biosystems Engineering, University of Minnesota, 1390 Eckles Ave., St. Paul, MN 55108, USA*

[g] *Department of Chemical and Biomolecular Engineering, The University of Tennessee, Knoxville, TN 37996, USA*

[h] *Biosciences Division, Oak Ridge National Laboratory, Oak Ridge, TN 37831, USA*

[i] *Korea Biochar Research Center, APRU Sustainable Waste Management & Division of Environmental Science and Ecological Engineering, Korea University, Seoul, 02841, Republic of Korea*

[j] *Department of Civil and Environmental Engineering, The Hong Kong Polytechnic University, Hung Hom, Kowloon, Hong Kong, China.*

* Corresponding author.

E-mail address: jiangjc@icifp.cn (J. Jiang); dan.tsang@polyu.edu.hk (D.C.W. Tsang)

Graphical Abstract

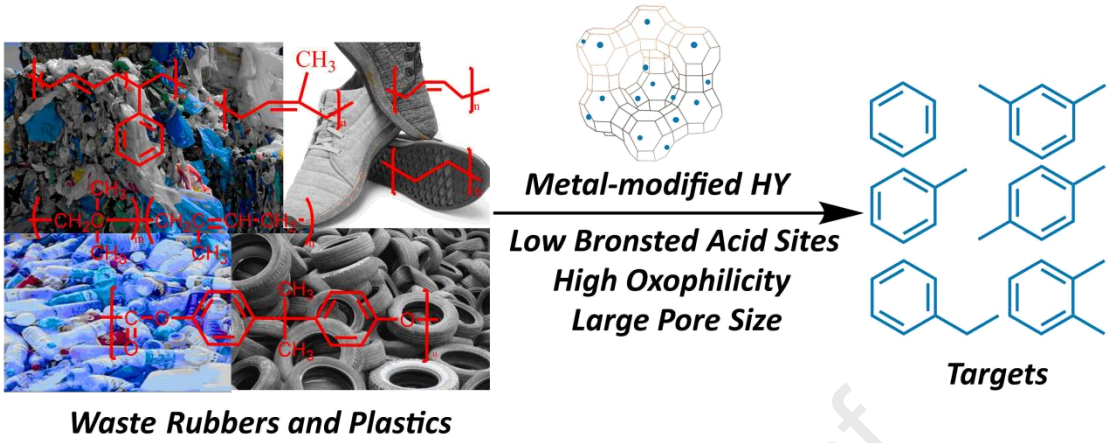

Catalytic degradation of waste rubbers and plastics over zeolites to produce aromatic hydrocarbons

Jia Wang [a, b], Jianchun Jiang [a, b], Xiaobo Wang [c], Mi Li [d], Yunjuan Sun [b], Shusheng Pang [e], Roger Ruan [f], Arthur J. Ragauskas [d, g, h], Yong Sik Ok [i], Daniel C.W. Tsang [j*]*

[a] *Jiangsu co-Innovation Center for Efficient Processing and Utilization of Forest Resources, College of Chemical Engineering, Nanjing Forestry University, Longpan Road 159, Nanjing 210037, China*

[b] *Institute of Chemical Industry of Forest Products, Chinese Academy of Forestry (CAF), No. 16, Suojin Five Village, Nanjing 210042, China*

[c] *School of Environmental Science, Nanjing Xiaozhuang University, Nanjing 211171, China*

[d] *Center for Renewable Carbon, Department of Forestry, Wildlife and Fisheries, The University of Tennessee, Knoxville, TN 37996, USA*

[e] *Department of Chemical and Process Engineering, University of Canterbury, Christchurch, New Zealand*

[f] *Center for Biorefining and Department of Bioproducts and Biosystems Engineering, University of Minnesota, 1390 Eckles Ave., St. Paul, MN 55108, USA*

[g] *Department of Chemical and Biomolecular Engineering, The University of Tennessee, Knoxville, TN 37996, USA*

[h] *Biosciences Division, Oak Ridge National Laboratory, Oak Ridge, TN 37831, USA*

[i] *Korea Biochar Research Center, APRU Sustainable Waste Management & Division of Environmental Science and Ecological Engineering, Korea University, Seoul, 02841, Republic of Korea*

[j] *Department of Civil and Environmental Engineering, The Hong Kong Polytechnic University, Hung Hom, Kowloon, Hong Kong, China.*

* Corresponding author.

E-mail address: jiangjc@icifp.cn (J. Jiang); dan.tsang@polyu.edu.hk (D.C.W. Tsang)

Abstract

Catalytic conversion of waste rubbers and plastics into aromatic hydrocarbons is a promising approach to waste management and energy recovery. In the present study, acidic HY zeolites were supported by cobalt, iron, and zirconium, and the catalysts were characterized by powder X-ray diffraction, nitrogen adsorption-desorption, ammonia temperature programmed desorption, X-ray photoelectron spectroscopy, and pyridine-Fourier transform infrared spectroscopy. The catalytic degradation of waste polybutadiene rubbers (BR) was conducted to investigate the degradation mechanism and evaluate the catalytic activity of supported zeolites. Experimental results indicated that HY loaded by zirconium and iron led to a higher content of Lewis acid sites as opposed to cobalt supported one. Compared with the non-catalytic pyrolysis of BR, the zirconium supported HY (Zr/HY) led to a 10-fold increase in aromatic hydrocarbons production with a distinctively high selectivity of 97.9%. A series of waste polymers including waste tires (WT), polyethylene (PE), polycarbonate (PC), and BR, were subjected to catalytic pyrolysis to explore the effects of polymer type on aromatic hydrocarbons generation, and BR was the most effective substrate, with yield enhancement reaching 2.4 over Zr/HY. Catalytic co-pyrolysis of waste rubbers and plastics was conducted to probe the effect of polymer structure on aromatic hydrocarbons formation, where a significant synergistic effect was observed in the PE co-fed with PC run.

Keywords

Catalytic pyrolysis; sustainable waste management; polybutadiene rubber; plastic recycling/valorization; aromatic hydrocarbons.

List of abbreviations

BR	Polybutadiene Rubbers	WT	Waste Tires
PE	Polyethylene	PC	Polycarbonate
XRD	X-ray Diffraction	NH_3-TPD	Ammonia-Temperature Programmed Desorption
Py-FTIR	Pyridine-Fourier Transform Infrared Spectroscopy	XPS	X-ray Photoelectron Spectroscopy
ICP-AES	Inductively Coupled Plasma-Atomic Emission Spectrometer	TIC	Total Ion Chromatogram
Py-GC/MS	Pyrolyzer- Gas Chromatography Coupled with Mass Spectrophotometry	S_{ch}	Relative Selectivity of Condensable Hydrocarbons
P_s	Area of Specific Component of Hydrocarbons	ΣP_{tc}	Total Area of Condensable Hydrocarbons
E_f	Yield Enhancement	$P_{s(i)}$	Area of Specific Components Obtained From Modified HY Zeolites Catalyzed Run
$P_{c(i)}$	Area Attained From Fresh HY Catalyzed Trial	P_h	Peak Area of a Certain Kind of Aromatics or Olefins
x_i	Mass Percentage of Hydrogen-Rich Materials in Feedstock Blends	x_{pc}	Mass Percentage of PC in Feedstock Blends
FAU	Faujasite Phase	B/L	Ratio of Brønsted to Lewis Acid Sites
AAs	C_{5+} Alkanes and Alkenes	AMHs	Aromatic Hydrocarbons
MAHs	Monocyclic Aromatic	C_5-C_9 GRs	Gasoline Range Products

	Hydrocarbons		
NIDs	Naphthalene and its Derivatives	BTEXAs	Enzene, Toluene, Ethylbenzene, Xylenes, and C_9 Alkylbenzenes
BTX	Benzene, Toluene, And Xylenes	H/C ratio	Hydrogen to Carbon Molar Ratio

1. Introduction

The extensive application of rubbers and plastics has led to a massive accumulation of solid wastes (Yousef et al., 2021). For example, the annual world potential of waste rubbers is 5.2 Mt for China, 3.3 Mt for Europe, 2.5 Mt for North America, and 1 Mt for Japan (Akkouche et al., 2018). Among the manufactured rubbers, synthetic polybutadiene rubber (BR) is a critical raw material that has been widely employed for cable insulation, automotive parts, and tire tread, accounting for 1/3 of rubber used in truck tires and 2/3 of rubber used in passenger car tires (Akkouche et al., 2018). Regarding the management of waste plastics, only 31.1% was recycled in European countries in 2016, while the EU directive on packaging wastes stipulates a recycling rate of 55% in 2030 (Schubert et al., 2020). Given the environmental protection regulations and renewable energy recovery targets, traditional methods such as incineration and landfilling are not suitable (Lee et al., 2020).

Pyrolysis is a thermochemical conversion process aiming at the production of liquid fuels, gases, and biochar (Wang, J. et al., 2020). It is well known that pyrolysis is more suitable for energy recovery from waste rubbers and/or plastics because of their chemical similarity to the petrochemical process of fossil-based feedstocks

(Darvishi et al., 2016). During the pyrolysis of waste rubbers or plastics, the long-chain hydrocarbons are degraded into smaller fragments, forming products with lower molecular weights which are more easily processed and upgraded (Kasar et al., 2020). However, the wide product distribution (i.e., carbon chain length goes up to C_{27}) limits the industrial application, and employing catalysts is a promising approach to upgrade the quality for downstream refinery (Kassargy et al., 2019).

A series of catalysts, including acidic zeolites and basic metal oxides, have been studied in the catalytic pyrolysis of waste polymers (Al-asadi et al., 2020). Compared with metal oxides, acidic zeolites are more effective in upgrading primary pyrolytic products (Chen et al., 2020). Among the zeolites, HY exhibited a more robust activity in generating single aromatic hydrocarbons such as toluene and xylenes, due to its larger pore size (i.e., 9.0 Å for USY, 7.8 Å for HY *vs.* 5.6 Å for HZSM-5). This structure allows the entrance of products with high molecular weights and favors the mass transfer (Kassargy et al., 2018). Our previous works indicated that compared with HZSM-5, HY and USY formed more monocyclic aromatic hydrocarbons in the catalytic pyrolysis of waste plastics (Wang et al., 2019). Moreover, Marcilla et al. (Marcilla et al., 2009) conducted the catalytic deconstruction of waste plastics over HY and HZSM-5, in which C_4 ~ C_{12} hydrocarbons were main products in the HY catalysis, while C_3 ~ C_6 fractions dominated the product distribution in the presence of HZSM-5.

Besides the textural property of zeolites, the acidic feature is also essential to aromatic hydrocarbons production (Ro et al., 2018). In general, a carbenium

92 mechanism induced by acid sites is responsible for the generation of primary radicals
93 via β-scission and hydrogen transfer reactions (Kim et al., 2017). Specifically, the
94 Brønsted acid sites facilitated cracking, oligomerization, and cyclization reactions,
95 while the Lewis acid sites were more effective for hydrogen transfer (such as
96 dehydrogenation and aromatization) (Bi et al., 2020). Therefore, tailoring the
97 Brønsted/Lewis acidity plays a vital role in the catalytic decomposition of polymers.
98 In this sense, an introduction of metal oxides into zeolites is an effective and efficient
99 approach (Al-asadi et al., 2020). For example, Han et al. (Han et al., 2021) explored
100 the catalytic pyrolysis mechanism of natural rubber over Zn-modified ZSM-5
101 catalysts, where they observed that 3% Zn loading exhibited the best selectivity to
102 aromatic hydrocarbons (~20%). However, to our best knowledge, the effect of metal
103 oxides supported HY on the catalytic pyrolysis of polybutadiene rubber, with an
104 emphasis on the generation of aromatic hydrocarbons, has not been studied.

105 In the present study, HY zeolites were supported by Co, Fe, and Zr, and X-ray
106 diffraction (XRD), N_2-adsorption/desorption, ammonia-temperature programmed
107 desorption (NH_3-TPD), X-ray photoelectron spectroscopy (XPS), and
108 pyridine-Fourier Transform Infrared Spectroscopy (Py-FTIR) were used to
109 characterize these catalysts. Secondly, catalytic pyrolysis of polybutadiene rubber (BR)
110 over supported catalysts was conducted to probe its degradation mechanism and
111 evaluate the catalytic activity. Thirdly, typical solid wastes including waste tires (WT),
112 low-density polyethylene (PE), and polycarbonate (PC), were employed to study the
113 effect of polymer type on the production of aromatic hydrocarbons. Finally, catalytic

co-pyrolysis of waste rubbers and plastics over iron supported HY was also carried out to further explore the possible synergy in feedstock blends.

2. Materials and experiments

2.1. Materials

The powdered polymers were purchased from Shuang Fuxin and Huachuang Polymer Materials Company in Guangdong province, China. The elemental analysis was carried out, and the results are summarized in Table S1. The commercial HY zeolites with a SiO_2/Al_2O_3 molar ratio of 5.4 were provided by the Catalyst Plant of Nankai University, Tianjin, China. The metal oxides supported HY catalysts were prepared based on previous works (Li et al., 2016). Specifically, for the iron supported HY, 2.17 g $Fe(NO_3)_3 \cdot 9H_2O$ and 10 g powder HY were dissolved in the deionized water (70 mL) with magnetic stirring for 10 min at 50 ^oC. The mixture was dried at 120 ^oC for 6 h, then was calcined at 550 ^oC for 5 h in static air. The HY zeolites supported by different metal oxides were labeled as Co/HY, Fe/HY, and Zr/HY, respectively.

2.2 Characterization

The XRD patterns were investigated by Bruker D8 Advance using CuKα radiation, and the scanning range of 2θ was from 5^o to 90^o with a scanning rate of 10^o min^{-1}. Nitrogen adsorption-desorption was conducted by a Micromeritics ASAP 2460 adsorption instrument with nitrogen at 77K. The NH_3-TPD was carried out via a Micromeritics Autochem II 2920. The catalysts were pretreated (100 mg for each run)

under He at 450 °C for 1 h, and they were saturated with 10% NH_3/He (50 mL/min) at 100 °C for 1 h. Finally, the samples were purged with Ar (150 °C, 1 h), and the TPD was conducted from 100 to 800 ^oC at a heating rate of 10 °C/min. Moreover, Pyridine-FTIR (Thermo Nicolet 380, Thermo Scientific) analysis was carried out in the scanning range of 450-4000 cm^{-1}. The samples were pretreated at 350 °C for 1 h, then were cooled to 40 °C to record the background. The pyridine vapor was adsorbed for 30 min and was purged by N_2 for 30min, followed by the desorption for 1 h at the required temperature. X-ray photoelectron spectroscopy (XPS) was conducted on Thermo Fisher K-Alpha. The binding energy was calibrated using C 1s BE at 284.6 eV. The elemental analyses for Fe, Co, and Zr were determined by inductively coupled plasma-atomic emission spectrometer (ICP-AES) using an Agilent 725 instrument.

2.3 Experimental method

Catalytic pyrolysis of polymers was conducted via an analytical pyrolysis-gas chromatography/mass spectrometry (Py-GC/MS, CDS 5200-7890A/5975C, Agilent, Fig. 1). A quartz tube was used to load the feedstocks (fixed at 0.8 ± 0.01 mg). A catalyst to feedstock (C/F) mass ratio of 2:1 was used to ensure high contact efficiency of pyrolytic vapors and catalysts. In this sense, Park et al. (Park et al., 2019b) used a higher C/F of 5:1 to explore the co-feeding effect of waste plastic films on the catalytic degradation of *quercus variabilis* over HY and HZSM-5. The reaction temperature was controlled at 650 ^oC with a heating rate of 10 ^oC/ms, and the hold

time was 30 s. The identification of pyrolytic products was conducted by comparing mass spectra with the NIST MS library. The concentration of pyrolytic products was measured by the total ion chromatogram (TIC) area of identified peaks. Each experiment was at least duplicated, and the average values were reported.

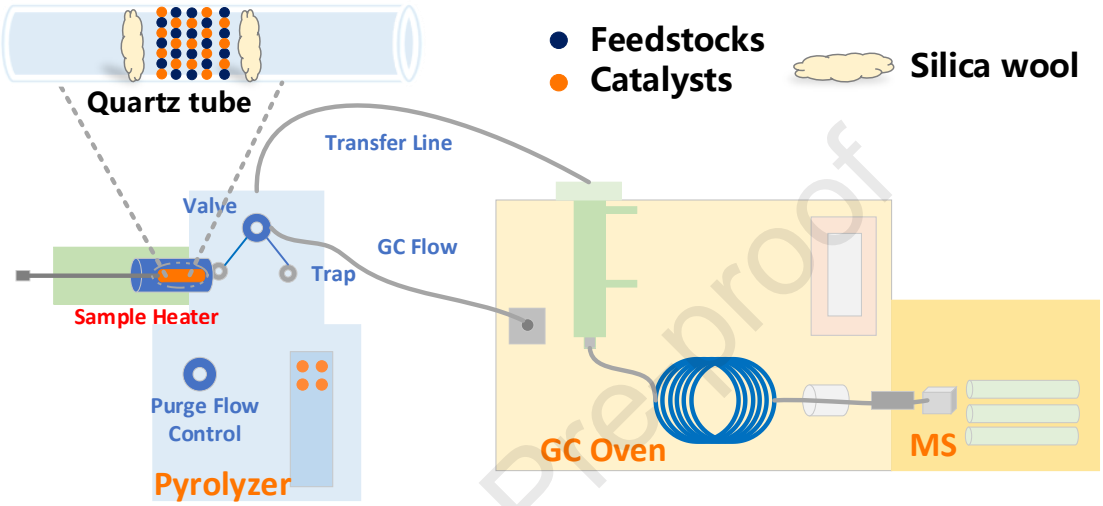

Fig. 1. Schematic diagram of the Py-GC/MS configuration.

The relative selectivity of condensable hydrocarbons (S_{ch}) was calculated as follows:

$$S_{ch} = \frac{P_s}{\sum P_{tc}} \quad (1)$$

where P_s is the area of a specific component of hydrocarbons, and ΣP_{tc} is the total area of condensable hydrocarbons.

To compare the catalytic activity of metal supported HY in terms of aromatic hydrocarbons generation, the enhancement factor was calculated based on the TIC area difference. In fact, for specific components such as alkenes or aromatic hydrocarbons, there is a linear relationship between the variations in the TIC area and its quantity. Therefore, the enhancement factor could be used to evaluate the catalytic

performance of modified HY due to it was calculated by employing the same control (i.e., the TIC area obtained from the standard HY). The equation is shown below:

$$E_f = \frac{p_{s(i)} - p_{c(i)}}{p_{c(i)}} \quad (2)$$

where $P_{s(i)}$ is the area of a specific component obtained from supported HY, $P_{c(i)}$ is the area attained from fresh HY.

The theoretical aromatic hydrocarbons and the synergistic effect during the co-pyrolysis of waste rubbers and plastics were calculated shown as below:

$$Theoretical_{(i,j)} = \frac{x_i A_j + x_{pc} A_{PC}}{x_i + x_{pc}} \quad (3)$$

$$Synergistic\ Effect = \frac{Experimental - Theoretical}{Theoretical} \times 100\% \quad (4)$$

where x_i (i = WT, BR, and PE) and x_{pc} are the mass percentages of hydrogen-rich materials and PC in feedstock blends, respectively. A_j (j = benzene, toluene, ethylbenzene, xylenes, and alkylbenzenes) is the area obtained from catalytic pyrolysis of pure hydrogen-rich materials, and A_{pc} is the corresponding area derived from pure PC degradation.

3 Results and Discussion

3.1 Catalyst characterization

3.1.1 Textural properties

Fig. 2a shows the XRD characterization results of studied catalysts. As indicated, the samples are characteristic of the faujasite phase (FAU, Fig. S1), suggesting that

191 the HY zeolite framework remained intact after introducing metal species. No distinct
192 characteristic peaks corresponding to metal species were identified, indicating that the
193 metals in the form of their respective oxides were dispersed well on the surface of HY
194 (Li et al., 2017). The element content of introduced metals was 3.1%, 3.1%, and 2.9%
195 for Co, Fe, and Zr, respectively (by ICP-AES). Nevertheless, the introduction of metal
196 species into HY led to a significant decrease in peak intensity compared with the
197 parent HY, which agreed with previous works (Zhang et al., 2019). The XPS spectra
198 is shown in Fig. 2b, as illustrated, for the Co 2p spectra, both Co^{2+} and Co^{3+} peaks
199 were observed, indicating the co-existence of CoO and Co_2O_3 on the Co/HY. A
200 similar trend was obtained for Fe 2p spectra as the content of Fe^{3+} and Fe^{2+} reached
201 56.7% and 43.3%, respectively. Concerning the Zr 3d spectra, only Zr^{4+} species were
202 attained on the surface of Zr/HY.

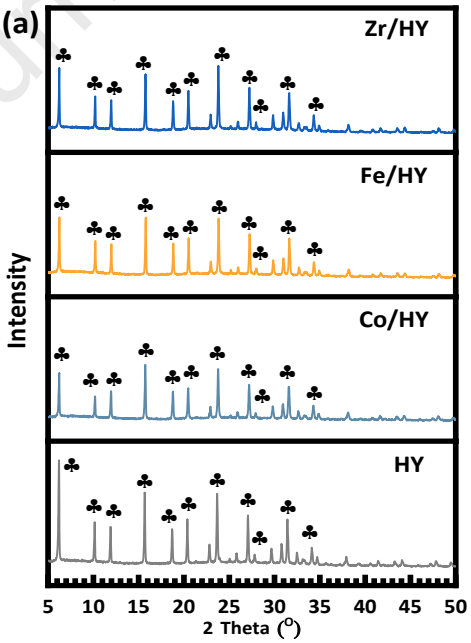

203

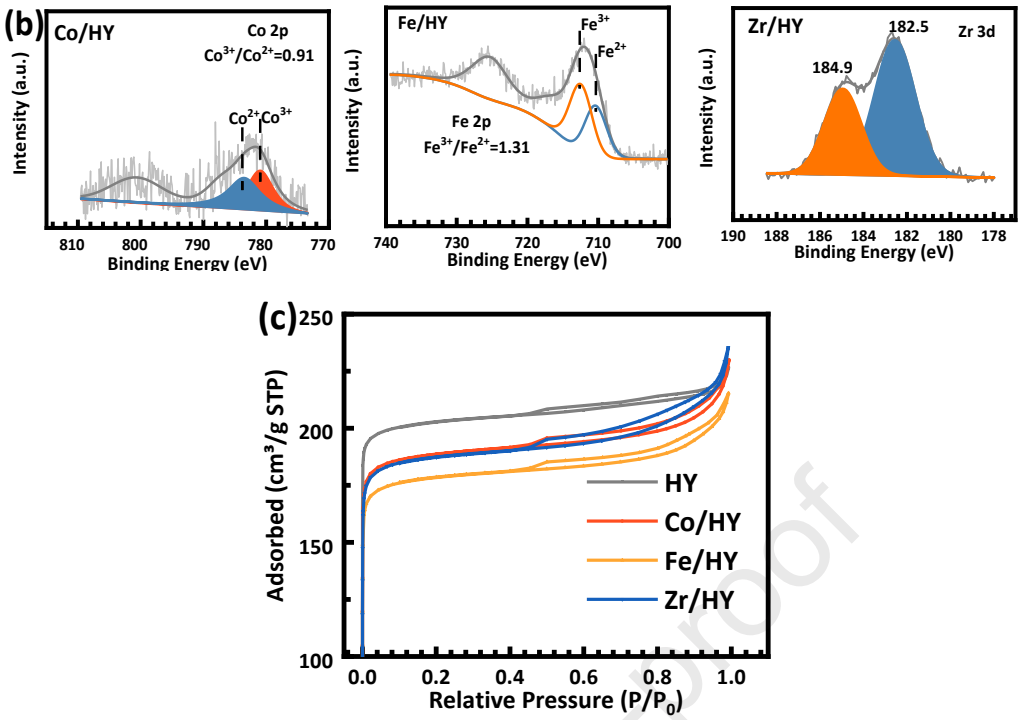

Fig. 2. X-ray diffractograms (a), XPS(b), and N_2 adsorption-desorption isotherms (c) of standard and modified HY.

Fig. 2c illustrates the N_2-adsorption/desorption isotherms of parent HY, Co/HY, Fe/HY, and Zr/HY, respectively (pore size distribution shown in Fig. S2). A typical type II isotherm, which is characteristic of microporous structure, was observed both in standard HY and metal supported ones (Wei et al., 2020). The textural properties, including total surface area, micropore area and pore volume, are summarized in Table 1. As shown, an addition of metal species into HY decreased the surface area. For instance, the surface area was 835 m^2/g for parent HY, while it decreased to 765 m^2/g for Co/HY, 723 m^2/g for Fe/HY, 759 m^2/g for Zr/HY, respectively. Similarly, the introduction of metal species also resulted in a slight decrease in pore volume. This data might be attributed to the presence of metal oxides aggregated on the surface or deposited into the pores of catalysts (Li et al., 2017).

219 Table 1 Textural properties of HY samples.

Sample	BET Surface area (m^2/g)	Micropore area[a] (m^2/g)	V_{total} [b] (cm^3/g)	V_{micro} [a] (cm^3/g)
HY	835	773	0.35	0.29
Co/HY	765	698	0.35	0.26
Fe/HY	723	663	0.33	0.25
Zr/HY	759	688	0.35	0.26

220 [a] By *t*-Plot; [b] Calculated at P/P_0= 0.990.

221 *3.1.2 Acidity of catalysts*

222 The acidic properties are characterized by NH_3-TPD. As indicated in Fig. 3a, for
223 the fresh HY, the desorption of ammonia took place from 100 to 600 ^oC, suggesting
224 that there was a wide range of acid sites in the parent HY. The desorption signal was
225 divided into two typical peaks centered at ~157 and ~400 ^oC, which represented the
226 sites of the weak and strong acidity, respectively. The concentration of total acid sites
227 was reduced from 0.72 mmol/g to 0.50 mmol/g for Co/HY, 0.57 mmol/g for Fe/HY,
228 and 0.62 mmol/g for Zr/HY, respectively (Table S2), which might be ascribed to the
229 preferential occupation of acid sites by metal species (Xu, Y. et al., 2018). An
230 introduction of metal species into HY decreased the percentage of strong acid sites
231 from 48.6% to 32.0%, 36.8%, and 29.0% for Co/HY, Fe/HY, and Zr/HY, respectively
232 (Fig. 3b). In contrast, modifying HY by loading Zr resulted in an increase in the weak
233 acid sites as its percentage reached 71% (*vs.* 51.4% for fresh HY).

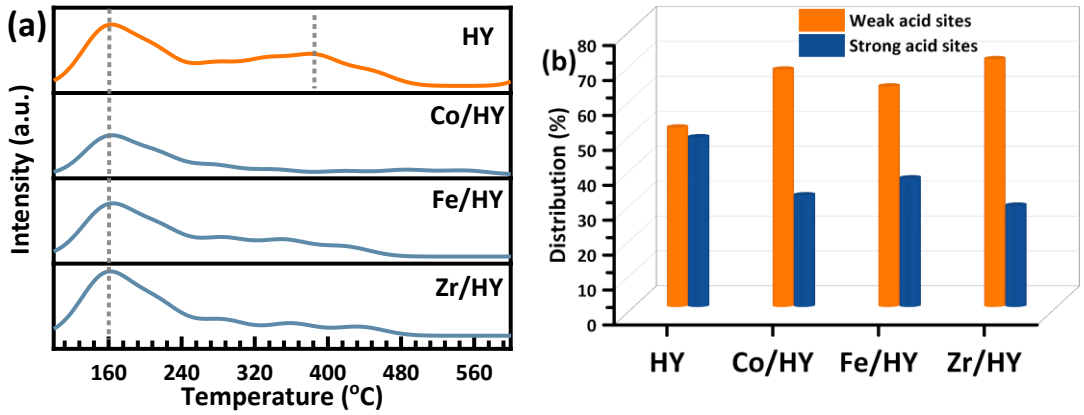

Fig. 3. NH_3-TPD profiles (a) and distribution of acid sites (b) of parent HY and supported HY zeolites.

The distribution of Brønsted and Lewis acidity was further studied by pyridine-FTIR. Generally, the absorption at *ca.* 1445-1454 cm^{-1} indicated the presence of Lewis acid sites, while the bands at ~1546 and ~1630 cm^{-1} were assigned to Brønsted acid sites (Zhang et al., 2019). As shown in Fig. 4, both Lewis and Brønsted acid sites were detected, and the amounts of Brønsted acid sites were reduced upon introducing metal species. For instance, the content of Brønsted acid sites decreased from 169.6 μmol/g for HY to 96.2 μmol/g for Co/HY, 106.8 μmol/g for Fe/HY, and 125.8 μmol/g for Zr/HY, whereas the amounts of Lewis acid sites increased from 60.1 μmol/g to 88.7 μmol/g for Zr/HY. Moreover, the ratio of Brønsted to Lewis acid sites (B/L) was calculated by normalizing peak areas at ~1546 and ~1454 cm^{-1}. Compared with fresh HY with a B/L ratio of 2.8, the Co/HY, Fe/HY, and Zr/HY decreased the B/L ratio to 1.6, 2.5, and 1.4, respectively.

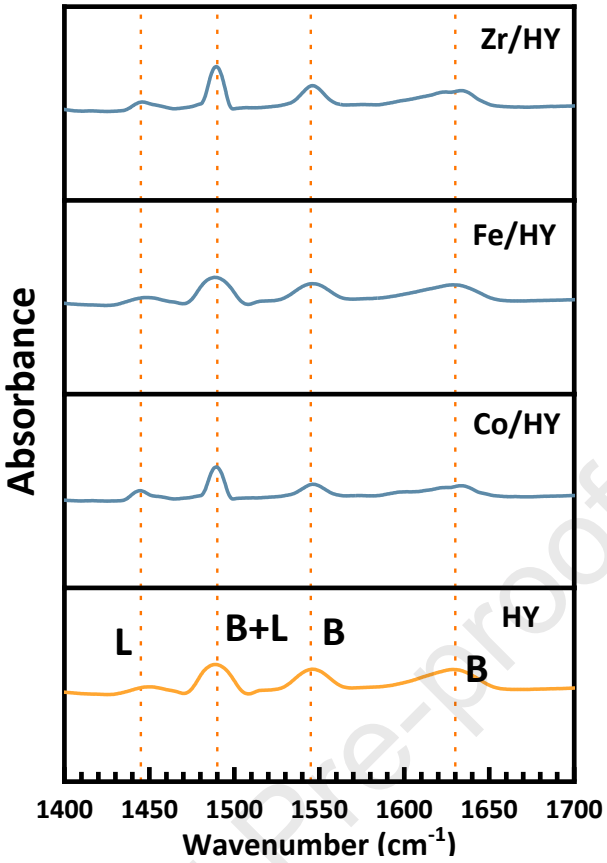

Fig. 4. Py-FTIR spectra obtained at 150 ^{o}C; B: Brønsted acid sites; L: Lewis acid sites.

3.2 Catalytic performance of supported HY in the degradation of BR

3.2.1 Comparison of non-catalytic and catalytic pyrolysis

Fig. 5 shows the components derived from catalytic pyrolysis of BR over fresh and supported HY. The non-catalytic (gray dashed line) was embedded to make a comparison. As indicated, the thermochemical conversion of BR produced a series of hydrocarbons, including C_4 olefins, C_{5+} alkanes and alkenes (AAs), and aromatic hydrocarbons (GC/MS chromatograms shown in Fig. 6). For the catalyst-free run, the product distribution was dominated by C_4 species (1,3-butadiene) followed by alkanes and alkenes, and only a limited aromatic hydrocarbons was generated (Fig. 5c). In

general, the degradation of BR follows a free radical mechanism, and the primary decomposition starts from the dissociation of the C-C single bond to form radicals (Gupte and Madras, 2004). These radicals were further rearranged to produce primary butadiene and 4-vinylcyclohexene. Subsequently, the formed 4-vinylcyclohexene undergoes dehydrogenation, dealkylation, and end group alkyl reaction to produce aromatic hydrocarbons because of its poor thermal stability (Sanglar et al., 2010). Choi and Kwon (Choi and Kwon, 2014) reported that the hydrogen transfer to the C=C bond takes place at high reaction temperature (>660 ^{o}C), resulting in the generation of long single carbon bond sequences (~C-C-C-C~) via 1,2 hydrogen followed by 1,5 hydrogen shifts. The produced single C bond sequences are easily broken to generate free radicals which are responsible for cyclic hydrocarbons. Therefore, the generation of aromatic hydrocarbons could be attributed to the dehydrogenation and dealkylation of cyclic hydrocarbons, as shown in Scheme 1.

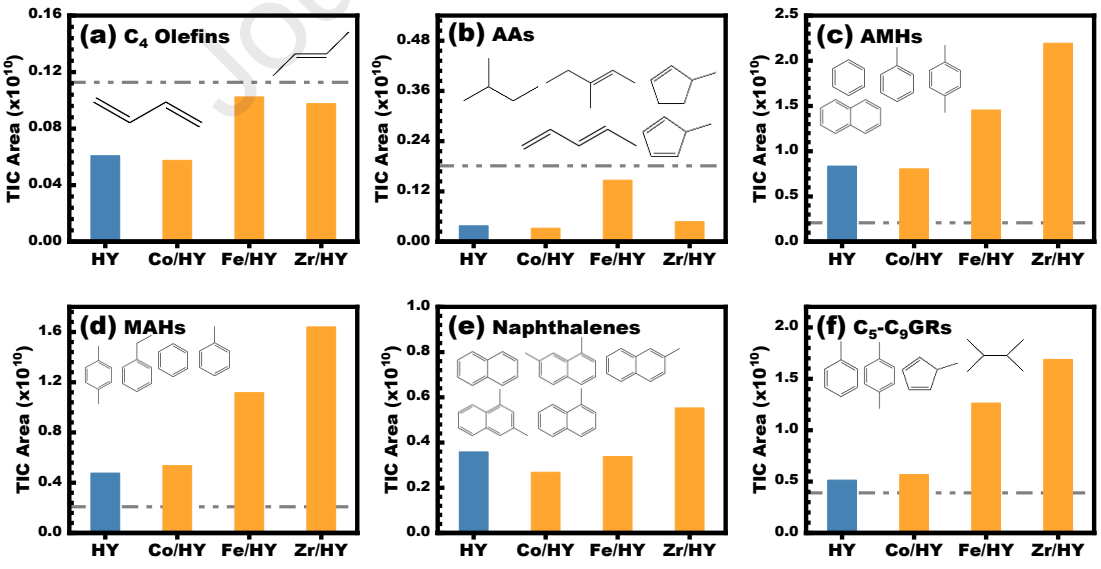

Fig. 5. Pyrolytic products obtained from catalytic degradation of BR as a function of catalyst type: AAs: alkanes and alkenes; AMHs: aromatic hydrocarbons; MAHs:

278 monocyclic aromatic hydrocarbons; C_5-C_9 GRs: gasoline range products.

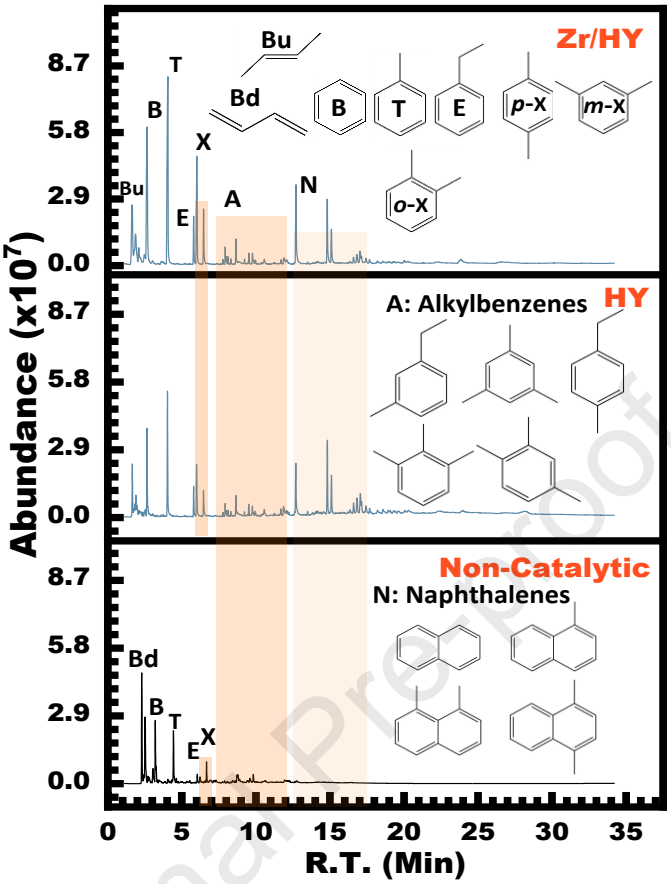

279

280 Fig. 6. GC/MS chromatograms obtained from catalytic degradation of BR.

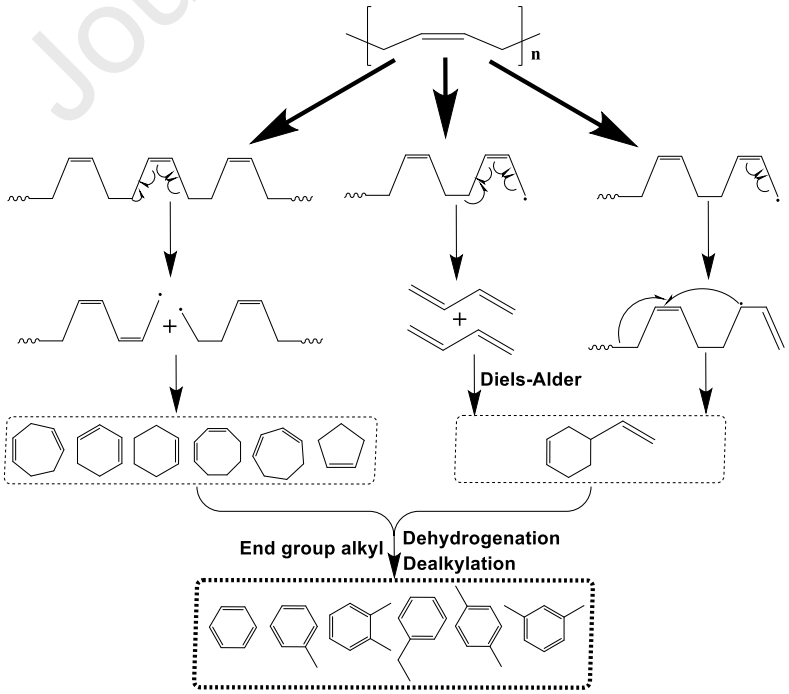

281

282 Scheme 1. From BR to aromatic hydrocarbons: Degradation pathway.

283 In the case of catalytic pyrolysis of BR over HY, compared with non-catalytic run,
284 the HY catalysis significantly affected the distribution of hydrocarbons, and a 4-fold
285 increase in aromatic hydrocarbons production was obtained (Fig. 5c). More
286 importantly, the selectivity of aromatic hydrocarbons reached 95.7% over HY (Fig. 7),
287 which was 56.5% higher than that of the non-catalytic. As previously mentioned, a
288 carbenium mechanism induced by acid sites in HY contributes to the primary radicals
289 by *β*-scission and hydrogen transfer (Akubo et al., 2019). Subsequently, the cracking,
290 oligomerization, aromatization, cyclization, and Diels-Alder reactions take place on
291 the active sites to produce aromatic hydrocarbons (Xu, F. et al., 2018). Furthermore,
292 the larger pore size of HY (7.8 Å *vs.* 5.6 Å for HZSM-5) gives an additional
293 advantage for accelerating the contact efficiency between bulky molecules and active
294 sites. For instance, Santos et al. (Santos et al., 2019) conducted catalytic pyrolysis of
295 plastic blends (PE and PP) over HZSM-5 and USY, in which the presence of weak
296 acid sites and large pore size in USY favored the degradation of plastics to yield more
297 liquid fraction. Moreover, the secondary reactions of alkenes (i.e., hydrocarbon pool
298 mechanism) to generate aromatic hydrocarbons were also promoted by zeolites (Wang,
299 Y. et al., 2020). Therefore, the enhanced aromatic hydrocarbons production was
300 accompanied by a significant decrease in C_4 olefins, alkanes, and alkenes, as shown in
301 Fig. 5a and 5b.

302 *3.2.2 Catalytic activity of supported HY zeolites*

303 Regarding the catalytic performance of supported HY in the catalytic

304 decomposition of BR, as illustrated in Fig. 5, Co/HY, Fe/HY, and Zr/HY produced
305 more aromatic monomers as opposed to the fresh HY. For instance, the enhancement
306 factor of monocyclic aromatic hydrocarbons (MAHs) reached 0.1 for Co/HY, 1.3 for
307 Fe/HY, and 2.4 for Zr/HY, respectively. A similar trend was observed for
308 gasoline-range hydrocarbons (GRs: mainly were C_5~C_9 alkenes and MAHs) as the
309 enhancement increased to 2.3 in the Zr/HY catalyzed run (*vs.* 0.1 for Co/HY and 1.5
310 for Fe/HY). Moreover, the selectivity to MAHs was 54.6% for HY, 64.1% for Co/HY,
311 69.7% for Fe/HY, and 73.2% for Zr/HY, respectively (Fig. 7).

312 Typically, the acidity properties of zeolites are crucial to aromatic hydrocarbons
313 formation (Özsin and Pütün, 2018). Compared with Brønsted acid sites which favored
314 the cracking, oligomerization, and cyclization reactions, the Lewis acid sites were
315 more effective in hydrogen transfer reactions such as dehydrogenation (Scheme 1)
316 (Choi and Kwon, 2014). It could be concluded that an increase in Lewis acid sites via
317 an introduction of metal species was beneficial. In the present work, a higher aromatic
318 hydrocarbons production in the Zr/HY catalyzed BR was attributed to its higher
319 content of Lewis acid sites (88.7 *vs.* 60.1 μmol/g for parent HY, Fig. 4). Furthermore,
320 the high surface area (759.0 m^2/g, Table 1) provides an additional advantage for
321 desirable aromatic hydrocarbons.

322 On the other hand, introducing active prompters such as Fe and Zr further enhanced
323 the catalytic activity by promoting hydrogen transfer reactions. For instance, Ma et al.
324 (Ma et al., 2018) explored the degradation mechanism of Br-ABS, where they
325 observed that the iron-based ZSM-5 benefited the depolymerization of polystyrene to

styrene by converting the thermally degraded carbo-radical to a carbanion. Hence, the improved aromatic hydrocarbons in the Fe/HY and Zr/HY catalyzed trials in this study might be ascribed to the coordination between Lewis acid sites and the iron or zirconium active species. Furthermore, compared with the parent HY, the Co, Fe, and Zr supported HY reduced the selectivity of naphthalene and its derivates (NIDs) which was related to the decrease in Brønsted acid sites (Fig. 4) (Rezaei et al., 2016). Specifically, the NIDs selectivity was 41.1% in HY, while it was decreased to 32.1%, 21.1%, and 24.7% when Co/HY, Fe/HY, and Zr/HY was used, respectively.

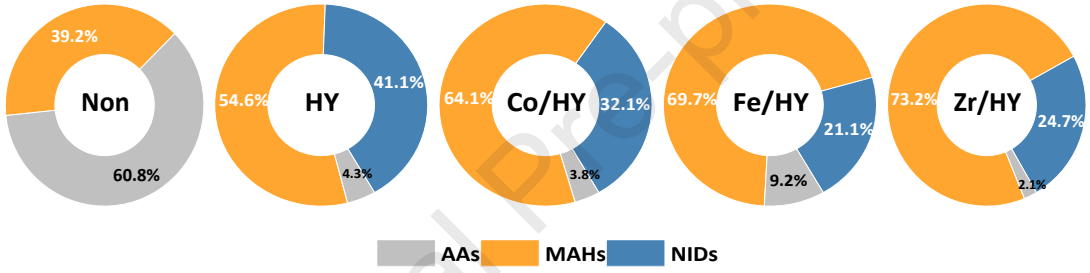

Fig. 7. Selectivity of condensable pyrolytic products obtained from non-catalytic and catalytic degradation of BR: AAs: Alkanes and alkenes; MAHs: monocyclic aromatic hydrocarbons; NIDs: naphthalene and its derivatives.

3.2.3 Distribution of monocyclic aromatic hydrocarbons (MAHs)

Concerning the distribution of MAHs (e.g., benzene, toluene, ethylbenzene, xylenes, and C9 alkylbenzenes, BTEXAs), as illustrated in Fig. 8, the distribution was mainly dominated by benzene, toluene, and xylenes (BTX). Employing zeolites (both fresh and modified ones) favored MAHs to different levels in comparison with the non-catalytic. Among the supported zeolites, Fe/HY and Zr/HY exhibited higher catalytic activity than Co/HY. For example, Zr/HY resulted in a 3.8-fold activity

increase in producing xylenes as opposed to Co/HY for BR degradation. This might be attributed to the lowest content of active acid sites in Co/HY (Table 1), which inhibited the hydrogen transfer reactions. Moreover, higher dehydrogenation and aromatization activities in Fe and Zr active species were also responsible for the enhanced production of targeted aromatic monomers (Akubo et al., 2019).

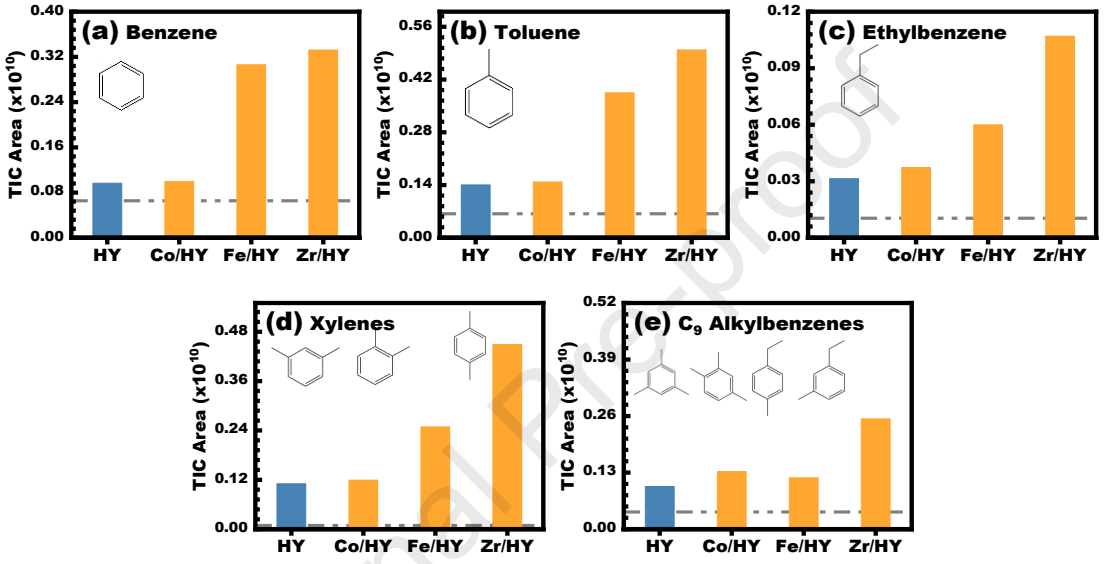

Fig. 8. Distribution of MAHs obtained from catalytic degradation of BR: Effect of catalyst type.

The selectivity of MAHs is summarized in Fig. 9. As indicated, toluene was the most abundant with a maximum value of 16.1% for standard HY catalyzed run, followed by xylenes. Employing supported HY resulted in an increased selectivity in BTX. More specifically, Fe/HY was the most active in improving the selectivity of benzene and toluene with a ~8% increase rate as opposed to the fresh HY. In comparison, Zr/HY was more beneficial to xylenes selectivity with a peak of 20.0%. It is well known that MAHs, particularly for BTX, are critical raw industrial materials with high market demand. For example, benzene is a raw feedstock for producing

cyclohexane, which is a nylon precursor (Gaurh and Pramanik, 2018). Toluene is widely employed as gasoline blending to improve the octane value. Xylenes (including *m*-, *o*-, and *p*-xylene) are widely used in producing plastic bottles and polyester clothing. Therefore, modifying HY by loading Fe and Zr to recycle these desirable aromatic monomers from waste rubbers and plastics, is beneficial for sustainable waste management and resource recycling.

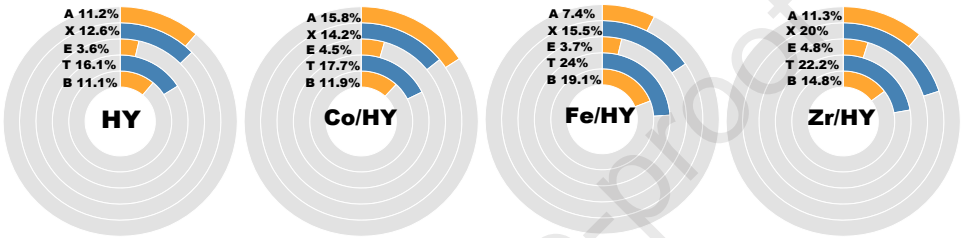

Fig. 9. Selectivity of BTEXAs derived from the catalytic conversion of BR as a function of catalyst type: B: benzene; T: toluene; E: ethylbenzene; X: xylenes; A: alkylbenzenes.

3.3 Further evaluation of modified HY in deconstruction of waste polymer blends

3.3.1 Effect of polymer type on aromatic hydrocarbons production

To verify whether the metal supported HY could exhibit superior catalytic activity in converting other waste polymers into aromatic hydrocarbons (in particular BTX), both waste rubbers and waste plastics including waste tires (WT), low-density polyethylene (PE), and polycarbonate (PC), were subjected to catalytic pyrolysis over Fe/HY and Zr/HY, respectively. Moreover, we also conducted the non-catalytic pyrolysis to explore how the polymer type affected the original distribution of pyrolytic products, and the experimental results are summarized in Figs. S3~S5. As

382 expected, polymer type significantly affected the distribution of pyrolytic
383 components. For example, alkanes and alkenes (AAs) were the predominant
384 fractions with a high concentration of 97.2%, 60.8%, and 49.8% in the degradation
385 of PE, BR, and WT, respectively. While the product distribution derived from the
386 thermochemical decomposition of PC was dominated by phenolic products (~70.1%,
387 mainly were phenol and cresols, Fig. S4a).

388 The products derived from catalytic decomposition of studied polymers is shown
389 in Fig. 10. Compared with the fresh HY, Fe/HY or Zr/HY enhanced the aromatic
390 hydrocarbons regardless of polymer type. For example, when Zr/HY was used as a
391 catalyst, the enhancement factor of MAHs was 0.6, 2.4, 0.3, and 0.4 for WT, BR, PE,
392 and PC, respectively. The selectivity of pyrolytic components was also highly
393 dependent on the introduced metal promoters. Taking the catalytic pyrolysis of PC for
394 instance, the Zr/HY and Fe/HY improved MAHs selectivity from 29.4% to 36.4% and
395 32.2%, respectively (Fig. S4a). Generally, pure acidic zeolites are not suitable for the
396 deoxygenation of phenolic products because these components have a high potential
397 to generate a strong bonding with acid sites on zeolites (such as HZSM-5, Hβ, and
398 HY), which leads to the catalyst deactivation (Rezaei et al., 2016). It is noteworthy
399 that introducing Fe and Zr with enhanced oxophilicity or oxygen vacancies facilitated
400 the deoxygenation of phenolic products (C-O bond cleavage) to form aromatic
401 hydrocarbons (Rezaei et al., 2016), and a similar trend was obtained in the present
402 study as the increased aromatic hydrocarbons was associated with a significant
403 decrease in phenols (~70.1% for non-catalytic *vs.* 63.3% for Fe/HY, 52.2% for

404 Zr/HY).

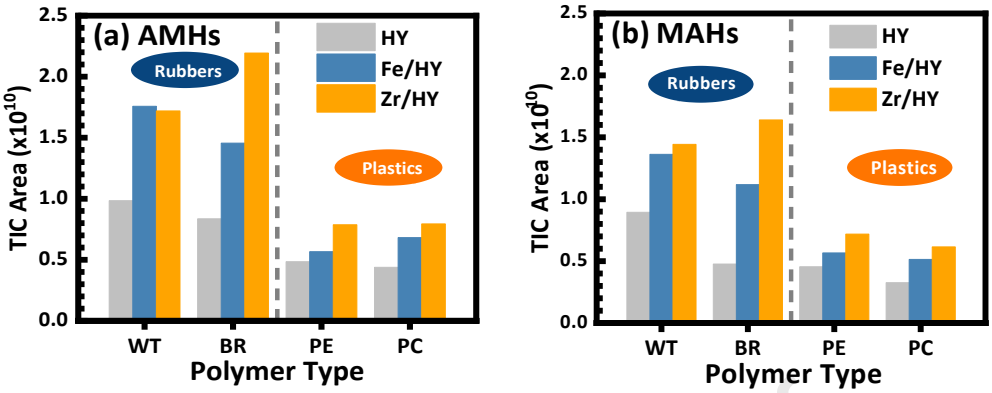

405

406 Fig. 10. Pyrolytic products obtained from catalytic degradation of polymers: AMHs:
407 aromatic hydrocarbons; MAHs: monocyclic aromatic hydrocarbons.

408 Concerning the effect of polymer structure on the BTX enhancement factors, waste
409 rubbers exhibited better activity in comparison with waste plastics (Figs. S6~S7).
410 Specifically, taking toluene for an example, the enhancement factor was 2.6 for BR
411 and 0.4 for PC over Zr/HY, indicating that Zr/HY exhibited over 6 times higher
412 catalytic activity in generating toluene compared with that of PC. The maximum
413 enhancement factors of BTX were also attained from Zr/HY catalyzed BR run. There
414 were no xylenes or alkylbenzenes formed in the catalytic pyrolysis of PC; conversely,
415 xylenes formation was maximized with a selectivity of 25.7% in the Zr/HY catalyzed
416 WT trial (Fig. S8).

417 *3.3.2 Effect of polymer blends on aromatic hydrocarbons production*

418 To further evaluate the catalytic performance of supported HY in the deconstruction
419 of polymer blends, we subsequently conducted the catalytic co-pyrolysis of waste
420 rubbers and plastics. During the catalytic pyrolysis, the generation of aromatic

hydrocarbons was significantly dependent on the H/C effective ratio of feedstocks, for example, Zhang et al. (Zhang et al., 2011) concluded that a higher H/C effective ratio favored aromatics and olefins production. Hence, PC was selected as the fundamental feedstock due to its lowest H/C effective ratio of 0.5 (*vs.* 2.0 for PE and 1.2 for BR, Table S1).

Fig. 11 shows the main pyrolytic products obtained from the Fe/HY catalyzed co-pyrolysis. As expected, co-feeding PC with hydrogen-rich materials reduced phenols. Specifically, the reduction rate reached 49.2%, 50.6%, and 73.1% when WT, BR, and PE was co-fed with PC, respectively. Conversely, elevating the H/C effective ratio via co-pyrolysis facilitated aromatic hydrocarbons to different levels, depending on the hydrogen-rich materials employed as shown in Fig. 11b. Moreover, the selectivity of aromatic hydrocarbons increased from 40.7% for pure PC to 66.8% for WT+PC, 63.4% for BR+PC, 63.9% for PE+PC, respectively (Fig. 12).

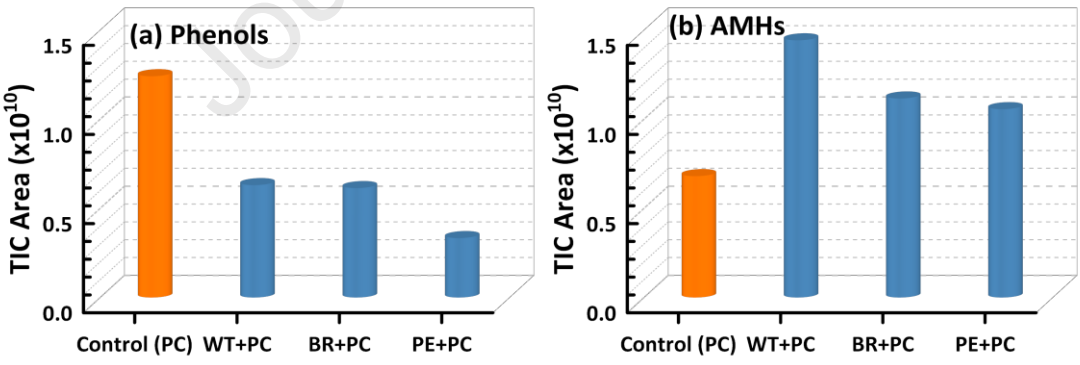

Fig. 11. Pyrolytic phenols (a) and aromatic hydrocarbons (b) attained from catalytic co-pyrolysis of PC with hydrogen-rich materials over Fe/HY.

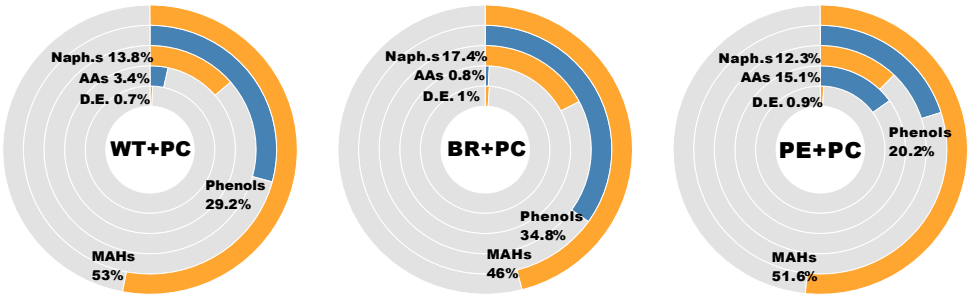

Fig. 12. Distribution of pyrolytic products derived from catalytic co-pyrolysis of PC with hydrogen-rich feedstocks over Fe/HY: MAHs: monocyclic aromatic hydrocarbons; Naph.s: Naphthalene and its derivatives; AAs: alkanes and alkenes; DE: diphenyl ether.

Regarding the distribution of MAHs, as shown in Fig. S9, BTX were the main components and their selectivity increased from 29.6% for pure PC to 38.3%, 35.6%, and 46.3% for PC+WT, PC+BR, and PC+PE, respectively. There could be a synergistic effect between feedstocks which facilitated the aromatic hydrocarbons production when the co-pyrolysis was conducted (Park et al., 2019a). To probe how this synergy affects the BTX formation, the theoretical BTX was calculated based on equation (3) and the results are summarized in Fig. S10. The synergistic effect that was calculated by equation (4) is illustrated in Fig. 13. As shown, a positive difference between experimental and theoretical BTX was observed in the PC co-fed with WT and PE, suggesting that a synergistic effect in BTX production was observed. Moreover, co-feeding PC with PE maximized this synergistic effect. Specifically, taking toluene for an example, the highest synergistic effect for its formation was 117.0% in PE co-pyrolyzed with PC (*vs.* 17.7% for WT+PC, -7.5% for BR+PC). This might be ascribed to the highest H/C effective ratio of PE (Table S1), which

maximized the synergistic effect to favor the increase of BTX.

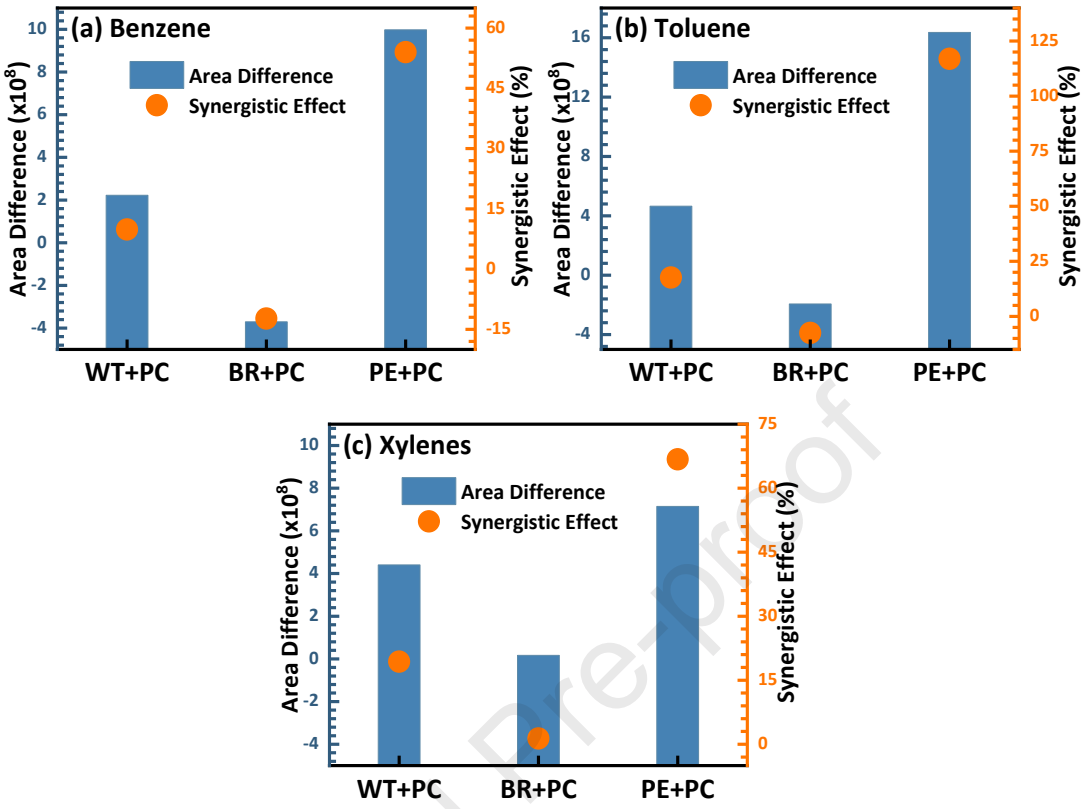

Fig. 13. Difference between experimental and theoretical BTX and the synergistic effect obtained from the co-pyrolysis.

3.3.3 Proposed reaction mechanism in the Fe/HY catalyzed co-pyrolysis process

In general, the hydrocarbon pool mechanism was responsible for aromatic hydrocarbons, and an increase in H/C effective ratio by co-pyrolysis further enhanced this mechanism to produce more desirable aromatics (Dorado et al., 2013). The phenolic compounds derived from PC degradation were stabilized by hydrogen transferred from hydrogen-rich feedstocks, and these stabilized phenolics were further deoxygenated via demethoxylation followed by dihydroxylation to generate aromatic hydrocarbons (Xue et al., 2016). Rezaei et al. (Rezaei et al., 2016) concluded that

zeolites with a lower percentage of strong acid sites and larger pore size are more appropriate for vapor upgrading of lignin-derived phenolic compounds. On the other hand, Zhang et al. (Zhang et al., 2020) reported that the higher oxophilicity of Fe results in a lower activation barrier for directly cleaving the C-O bond and increasing the aromatic hydrocarbons selectivity during the catalytic deoxygenation of phenolic products. Meanwhile, the oxophilic Fe was also calculated to interact preferably with phenoxy groups which promoted the direct C-O bond cleavage (Hensley et al., 2016). Hence, in the present study, modifying HY by loading Fe significantly decreased the strong acid sites from 0.35 mmol/g for parent HY to 0.21 mmol/g (Table S2). Meanwhile, a high content of Fe^{3+} with a value of 56.7% in Fe/HY (XPS results shown in Fig. 2c) also enhanced the oxophilicity to deoxygenate phenols. Furthermore, the channels of HY also provided an additional advantage for facilitating the diffusivity of phenolic molecules because its pore size (*ca.* 7.8 Å) was larger than the kinetic diameters of phenols (e.g., 5.5 Å for phenol, 5.9 Å for *o*-cresol, 6.0 Å for 2,3-xylenol, and 6.1 Å for anisole) (Rezaei et al., 2016). Therefore, the decrease in PC-derived phenols via the co-pyrolysis could be attributed to the synergy of Fe active promoters and the low content of strong acid sites, and a higher H/C effective ratio in feedstocks and the larger channels of HY further favored this synergy to deoxygenate phenols as proposed in Scheme 2. Moreover, we will scale up the degradation process and investigate the developed catalyst system via a two-step fixed bed reactor in our further work.

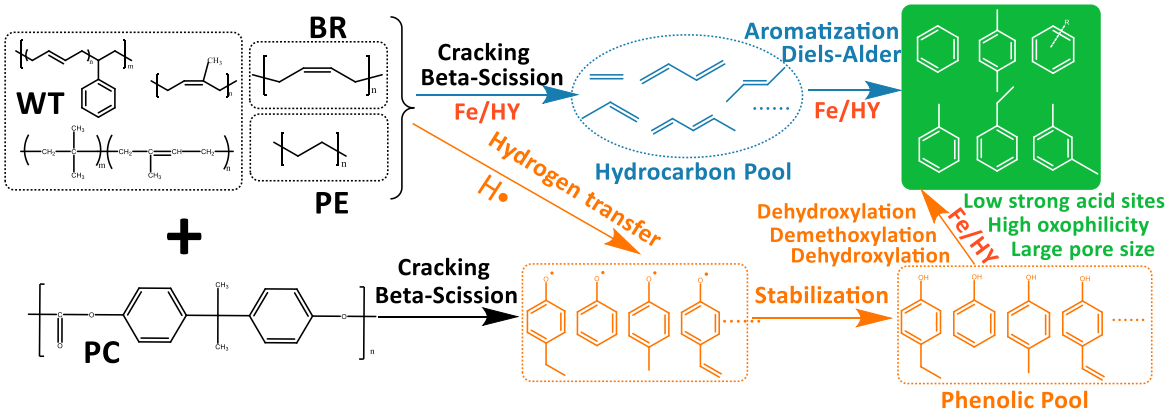

Scheme 2. Proposed reaction pathways for generating aromatic hydrocarbons during the co-pyrolysis of PC with hydrogen-rich materials.

4. Conclusions

In summary, introducing metal promoters into HY significantly affected the acidity property by lowering the amount of Brønsted acid sites. The catalytic performance of fresh and modified HY catalysts was tested in the catalytic pyrolysis of BR, and Zr/HY was more effective in forming aromatic hydrocarbons than the others. The product distribution of aromatic hydrocarbons was dominated by BTX, and Fe/HY was the most active in improving the selectivity of benzene and toluene with a ~8% increase rate, while Zr/HY was more beneficial to the xylene selectivity with a peak of 20.0%. The polymer type played a vital role in aromatic hydrocarbons generation, and catalytic degradation of waste rubbers produced more desirables than that of waste plastics. Among the studied polymers, BR was the most effective in forming aromatic hydrocarbons as the enhancement factor over Zr/HY was 0.6, 2.4, 0.3, and 0.4 for WT, BR, PE, and PC, respectively. There was a synergistic effect in feedstock

blends in the co-pyrolysis of waste rubbers and plastics which promoted the increase in desirable aromatics, and the highest synergistic effect for toluene formation was 117.0% in PE co-pyrolyzed with PC. Modifying HY zeolites by loading Fe or Zr to catalytically degrade waste rubbers and plastics is a promising approach to produce aromatic monomers for sustainable biorefinery.

Acknowledgments

The authors are grateful for the National Natural Science Foundation of China (No. 52006106), the Natural Science Foundation of Jiangsu Province (No. BK2020789), the China Postdoctoral Science Foundation (No. 2020TQ0154), and the Hong Kong Research Grants Council (PolyU 15217818).

Appendix A. Supplementary material

Supplementary data associated with this article can be found.

References

Akkouche, N., Balistrou, M., Loubar, K., Kadi, M.E.A., Tazerout, M., 2018. Pyrolysis Polybutadiene Model Including Self-Heating and Self-Cooling Effects: Kinetic Study via Particle Swarm Optimization. Waste and Biomass Valorization 11(2), 653-667.

Akubo, K., Nahil, M.A., Williams, P.T., 2019. Aromatic fuel oils produced from the pyrolysis-catalysis of polyethylene plastic with metal-impregnated zeolite catalysts. Journal of the Energy Institute 92(1), 195-202.

Al-asadi, M., Miskolczi, N., Eller, Z., 2020. Pyrolysis-gasification of wastes plastics for syngas production using metal modified zeolite catalysts under different ratio of nitrogen/oxygen. Journal of Cleaner Production 271.

Bi, C., Wang, X., You, Q., Liu, B., Li, Z., Zhang, J., Hao, Q., Sun, M., Chen, H., Ma, X., 2020. Catalytic upgrading of coal pyrolysis volatiles by Ga-substituted mesoporous ZSM-5. Fuel 267.

Chen, Z., Zhang, X., Che, L., Peng, H., Zhu, S., Yang, F., Zhang, X., 2020. Effect of volatile reactions on oil production and composition in thermal and catalytic pyrolysis of polyethylene. Fuel 271.

Choi, S.-S., Kwon, H.-M., 2014. Analytical method for determination of butadiene and styrene contents of styrene-butadiene rubber vulcanizates without pretreatment using pyrolysis-gas chromatography/mass spectrometry. Polym. Test. 38, 87-90.

Darvishi, A., Davand, R., Khorasheh, F., Fattahi, M., 2016. Modeling-based optimization of a fixed-bed industrial reactor for oxidative dehydrogenation of propane. Chin. J. Chem. Eng. 24(5), 612-622.

Dorado, C., Mullen, C.A., Boateng, A.A., 2013. H-ZSM5 Catalyzed Co-Pyrolysis of Biomass and Plastics. ACS Sustainable Chemistry & Engineering 2(2), 301-311.

Gaurh, P., Pramanik, H., 2018. Production of benzene/toluene/ethyl benzene/xylene (BTEX) via multiphase catalytic pyrolysis of hazardous waste polyethylene using low cost fly ash synthesized natural catalyst. Waste Manag 77, 114-130.

Gupte, S.L., Madras, G., 2004. Catalytic degradation of polybutadiene. Polym. Degradation Stab. 86(3), 529-533.

Han, Y., Yu, J., Chen, T., Liu, X., Sun, L., 2021. Study on catalytic pyrolysis mechanism of natural rubber (NR) over Zn-modified ZSM5 catalysts. Journal of the Energy Institute 94, 210-221.

Hensley, A.J.R., Wang, Y., McEwen, J.-S., 2016. Adsorption of guaiacol on Fe (110) and Pd (111) from first principles. SurSc 648, 227-235.

Kasar, P., Sharma, D.K., Ahmaruzzaman, M., 2020. Thermal and catalytic decomposition of waste plastics and its co-processing with petroleum residue through pyrolysis process. Journal of Cleaner Production 265.

Kassargy, C., Awad, S., Burnens, G., Kahine, K., Tazerout, M., 2018. Gasoline and diesel-like fuel production by continuous catalytic pyrolysis of waste polyethylene and polypropylene mixtures over USY zeolite. Fuel 224, 764-773.

Kassargy, C., Awad, S., Burnens, G., Upreti, G., Kahine, K., Tazerout, M., 2019. Study of the effects of regeneration of USY zeolite on the catalytic cracking of polyethylene. Applied Catalysis B: Environmental 244, 704-708.

Kim, Y.-M., Han, T.U., Kim, S., Jae, J., Jeon, J.-K., Jung, S.-C., Park, Y.-K., 2017. Catalytic co-pyrolysis of epoxy-printed circuit board and plastics over HZSM-5 and HY. Journal of Cleaner Production 168, 366-374.

Lee, T., Jung, S., Park, Y.K., Kim, T., Wang, H., Moon, D.H., Kwon, E.E., 2020. Catalytic Pyrolysis of Polystyrene over Steel Slag under CO2 Environment. J. Hazard. Mater. 395, 122576.

Li, P., Chen, X., Wang, X., Shao, J., Lin, G., Yang, H., Yang, Q., Chen, H., 2017. Catalytic Upgrading of Fast Pyrolysis Products with Fe-, Zr-, and Co-Modified Zeolites Based on Pyrolyzer–GC/MS Analysis. Energy Fuels 31(4), 3979-3986.

Li, P., Li, D., Yang, H., Wang, X., Chen, H., 2016. Effects of Fe-, Zr-, and Co-Modified Zeolites and Pretreatments on Catalytic Upgrading of Biomass Fast Pyrolysis Vapors. Energy Fuels 30(4), 3004-3013.

Ma, C., Yu, J., Chen, T., Yan, Q., Song, Z., Wang, B., Sun, L., 2018. Influence of Fe based ZSM-5 catalysts on the vapor intermediates from the pyrolysis of brominated

acrylonitrile-butadiene-styrene copolymer (Br-ABS). Fuel 230, 390-396.
Marcilla, A., Beltrán, M.I., Navarro, R., 2009. Thermal and catalytic pyrolysis of polyethylene over HZSM5 and HUSY zeolites in a batch reactor under dynamic conditions. Applied Catalysis B: Environmental 86(1-2), 78-86.
Özsin, G., Pütün, A.E., 2018. A comparative study on co-pyrolysis of lignocellulosic biomass with polyethylene terephthalate, polystyrene, and polyvinyl chloride: Synergistic effects and product characteristics. Journal of Cleaner Production 205, 1127-1138.
Park, Y.-K., Jung, J., Ryu, S., Lee, H.W., Siddiqui, M.Z., Jae, J., Watanabe, A., Kim, Y.-M., 2019a. Catalytic co-pyrolysis of yellow poplar wood and polyethylene terephthalate over two stage calcium oxide-ZSM-5. ApEn 250, 1706-1718.
Park, Y.-K., Lee, B., Lee, H.W., Watanabe, A., Jae, J., Tsang, Y.F., Kim, Y.-M., 2019b. Co-feeding effect of waste plastic films on the catalytic pyrolysis of Quercus variabilis over microporous HZSM-5 and HY catalysts. Chem. Eng. J. 378.
Rezaei, P.S., Shafaghat, H., Daud, W.M.A.W., 2016. Aromatic hydrocarbon production by catalytic pyrolysis of palm kernel shell waste using a bifunctional Fe/HBeta catalyst: effect of lignin-derived phenolics on zeolite deactivation. Green Chem. 18(6), 1684-1693.
Ro, D., Kim, Y.-M., Lee, I.-G., Jae, J., Jung, S.-C., Kim, S.C., Park, Y.-K., 2018. Bench scale catalytic fast pyrolysis of empty fruit bunches over low cost catalysts and HZSM-5 using a fixed bed reactor. Journal of Cleaner Production 176, 298-303.
Sanglar, C., Nguyen Quoc, H., Grenier-Loustalot, M.F., 2010. Studies on thermal degradation of 1-4 and 1-2 polybutadienes in inert atmosphere. Polym. Degradation Stab. 95(9), 1870-1876.
Santos, B.P.S., Almeida, D.D., Marques, M.d.F.V., Henriques, C.A., 2019. Degradation of Polypropylene and Polyethylene Wastes Over HZSM-5 and USY Zeolites. CatL 149(3), 798-812.
Schubert, T., Lechleitner, A., Lehner, M., Hofer, W., 2020. 4-Lump kinetic model of the co-pyrolysis of LDPE and a heavy petroleum fraction. Fuel 262.
Wang, J., Jiang, J., Meng, X., Li, M., Wang, X., Pang, S., Wang, K., Sun, Y., Zhong, Z., Ruan, R., Ragauskas, A.J., 2020. Promoting Aromatic Hydrocarbon Formation via Catalytic Pyrolysis of Polycarbonate Wastes over Fe- and Ce-Loaded Aluminum Oxide Catalysts. Environ Sci Technol 54(13), 8390-8400.
Wang, J., Jiang, J., Sun, Y., Zhong, Z., Wang, X., Xia, H., Liu, G., Pang, S., Wang, K., Li, M., Xu, J., Ruan, R., Ragauskas, A.J., 2019. Recycling benzene and ethylbenzene from in-situ catalytic fast pyrolysis of plastic wastes. Energy Convers. Manage. 200.
Wang, Y., Ke, L., Peng, Y., Yang, Q., Du, Z., Dai, L., Zhou, N., Liu, Y., Fu, G., Ruan, R., Xia, D., Jiang, L., 2020. Characteristics of the catalytic fast pyrolysis of vegetable oil soapstock for hydrocarbon-rich fuel. Energy Convers. Manage. 213.
Wei, B., Jin, L., Wang, D., Shi, H., Hu, H., 2020. Catalytic upgrading of lignite pyrolysis volatiles over modified HY zeolites. Fuel 259.
Xu, F., Wang, B., Yang, D., Ming, X., Jiang, Y., Hao, J., Qiao, Y., Tian, Y., 2018. TG-FTIR and Py-GC/MS study on pyrolysis mechanism and products distribution of waste bicycle tire. Energy Convers. Manage. 175, 288-297.

620 Xu, Y., Liu, J., Ma, G., Wang, J., Lin, J., Wang, H., Zhang, C., Ding, M., 2018. Effect
621 of iron loading on acidity and performance of Fe/HZSM-5 catalyst for direct synthesis
622 of aromatics from syngas. Fuel 228, 1-9.
623 Xue, Y., Kelkar, A., Bai, X., 2016. Catalytic co-pyrolysis of biomass and polyethylene
624 in a tandem micropyrolyzer. Fuel 166, 227-236.
625 Yousef, S., Eimontas, J., Zakarauskas, K., Striūgas, N., 2021. Microcrystalline
626 paraffin wax, biogas, carbon particles and aluminum recovery from metallised food
627 packaging plastics using pyrolysis, mechanical and chemical treatments. Journal of
628 Cleaner Production 290.
629 Zhang, H., Cheng, Y.-T., Vispute, T.P., Xiao, R., Huber, G.W., 2011. Catalytic
630 conversion of biomass-derived feedstocks into olefins and aromatics with ZSM-5: the
631 hydrogen to carbon effective ratio. Energy Environ. Sci. 4(6), 2297.
632 Zhang, H., Yang, W., Roslan, I.I., Jaenicke, S., Chuah, G.-K., 2019. A combo Zr-HY
633 and Al-HY zeolite catalysts for the one-pot cascade transformation of
634 biomass-derived furfural to γ-valerolactone. JCat 375, 56-67.
635 Zhang, J., Sun, J., Wang, Y., 2020. Recent advances in the selective catalytic
636 hydrodeoxygenation of lignin-derived oxygenates to arenes. Green Chem. 22(4),
637 1072-1098.
638

Highlights:

- Waste rubbers and plastics could be valorized into aromatic hydrocarbons.
- Introducing Co, Fe, and Zr into HY zeolites decreased the amounts of Brønsted acid sites.
- A ten-fold increase in yield with high selectivity of 97.9% was obtained over Zr/HY.
- Catalytic pyrolysis of waste rubbers produced more aromatic hydrocarbons.
- Co-pyrolysis of selected wastes showed synergistic production of aromatic hydrocarbons.

Declaration of interests

☒ The authors declare that they have no known competing financial interests or personal relationships that could have appeared to influence the work reported in this paper.

☐The authors declare the following financial interests/personal relationships which may be considered as potential competing interests: